

Discrete solitons in zigzag waveguide arrays with different types of linear mixing between nearest-neighbor and next-nearest-neighbor couplings

Jinzhou Hu^{1,§}, Shulan Li^{1,§}, Zhaopin Chen², Jiantao Lü¹, Bin Liu^{1*} and Yongyao Li^{1,2}

¹*School of Physics and Optoelectronic Engineering, Foshan University, Foshan 528000, China*

²*Department of Physical Electronics, School of Electrical Engineering, Faculty of Engineering, Tel Aviv University, Tel Aviv 69978, Israel and*

[§] *These authors contributed equally to this work.*

We study discrete solitons in zigzag discrete waveguide arrays with different types of linear mixing between nearest-neighbor and next-nearest-neighbor couplings. The waveguide array is constructed from two layers of one-dimensional (1D) waveguide arrays arranged in zigzag form. If we alternately label the number of waveguides between the two layers, the cross-layer couplings (which couple one waveguide in one layer with two adjacent waveguides in the other layer) construct the nearest-neighbor couplings, while the couplings that couple this waveguide with the two nearest-neighbor waveguides in the same layer, i.e., self-layer couplings, contribute the next-nearest-neighbor couplings. Two families of discrete solitons are found when these couplings feature different types of linear mixing. As the total power is increased, a phase transition of the second kind occurs for discrete solitons in one type of setting, which is formed when the nearest-neighbor coupling and next-nearest-neighbor coupling feature positive and negative linear mixing, respectively. The mobilities and collisions of these two families of solitons are discussed systematically throughout the paper, revealing that the width of the soliton plays an important role in its motion. Moreover, the phase transition strongly influences the motions and collisions of the solitons.

I. INTRODUCTION

The transmission of light fields in discrete systems manifests abundant functional phenomena [1]. Discrete waveguide arrays represent the most essential and fundamental element for discrete optics [2]. Diffraction management [3], including anomalous refraction, negative refraction, Anderson location [4], and Bloch oscillation [5], have been reported experimentally in discrete waveguide arrays. Another important phenomenon in nonlinear optical waveguide arrays is produced by the self-trapping of light, namely, discrete solitons, which are created through a balance between discrete diffraction effects and nonlinearity [6–18]. Discrete solitons in nonlinear waveguide array networks can provide an ideal platform for all-optical data processing applications and can achieve intelligent functional operations such as routing, blocking, logic functions, and time-gating [19]. Hence, discrete waveguide arrays are important devices for all-optical switching networks, similar to semiconductor devices in electronic circuits, and the discrete solitons in different functional discrete waveguide systems constitute an active topic in optics.

Generally, the tunneling of the light field among different waveguides originates from the evanescent coupling between adjacent (i.e., nearest-neighbor) waveguides, whereas the evanescent coupling between next-nearest-neighbor waveguides can be neglected. Hence, the propagation of a light field in this kind of waveguide array is always described by the discrete nonlinear Schrödinger equation (DNSE) with only first-order dis-

crete diffraction. However, it was reported that next-nearest-neighbor coupling was excited by the hopping of the light field in zigzag waveguide arrays [20–24]. Long-range coupling is introduced because a zigzag arrangement enhances the hopping rate of the light field to the next-nearest-neighbor site, and the propagation of a light field in zigzag waveguide arrays can be described by the DNSE with second-order discrete diffraction. Recently, a discrete waveguide array with an exponentially long range coupled effect was reported to be realized with the special design of the waveguide system [25, 26]. Because the coupling between the waveguides indicates a transition of energy, it always features negative linear mixing in the field between two connecting waveguides. In comparison, the coupling featuring positive linear mixing between two connecting waveguides has rarely been discussed. Recently, the synthetic (artificial) gauge field or complex coupling, which makes the coupling constant a complex number, was introduced into optical systems [27–32], allowing the coupling between two connecting waveguides to be tuned to feature either negative or positive linear mixing.

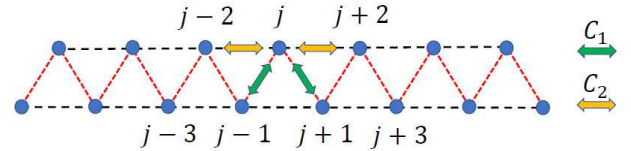


FIG. 1: Sketch of the zigzag waveguide arrays. Here, C_1 and C_2 denote the nearest-neighbor and next-nearest-neighbor couplings, respectively. In this model, these two couplings satisfy $C_1 \cdot C_2 < 0$.

*Electronic address: binliu@fosu.edu.cn

In this paper, we consider the zigzag waveguide system shown in Fig. 1. This waveguide array is formed by two layers of one-dimensional (1D) waveguide arrays. The waveguide in one layer constructs an equilateral triangle with the two adjacent waveguides of the other layers. If we alternately label the number of waveguides between two layers of the waveguides, which are ordered in the same sequence as in Ref. [20], the cross-core couplings, which couple one waveguide in one layer with the two adjacent waveguides in the neighboring layer, construct the nearest-neighbor coupling. In contrast, the self-core couplings, which couple the waveguide in one layer with the two nearest-neighbor waveguides in the same layers, contribute next-nearest-neighbor couplings. By introducing the synthetic gauge field into the coupling coefficient, we assume that these two types of couplings, i.e., cross-coupling and self-coupling, feature opposite types of linear mixing (i.e., negative and positive linear mixing) between the waveguides that are coupled. Hence, the aim of this paper is to study the characteristics, mobilities, and interactions of discrete solitons modulated by the opposite linear mixing between these two types of coupling. The rest of the paper is structured as follows: the model is described in Section II, the analysis and numerical results of the stationary solution and the dynamics of the discrete solitons are presented in Sections III and IV, respectively, and the conclusions are drawn in Section V.

II. THE MODEL

The settings of our model are illustrated in Fig. 1. The zigzag waveguide is formed by two layers of 1D waveguide arrays. The waveguide in one layer constructs an equilateral triangle with the two adjacent waveguides of the other layers. The sequence of the waveguide number is defined as the sketch, which follows the same definition as in Ref. [20]. Hence, the nearest-neighbor couplings for a waveguide in one layer, namely, C_1 , are contributed from the two adjacent waveguides in the neighboring layer, while the next-nearest-neighbor couplings, namely, C_2 , are contributed from the closest neighbor waveguides in the same layer. We assume that these waveguides feature self-focusing Kerr nonlinearity. The Hamiltonian of this system, in scaled form, is defined as [20]

$$H = \frac{1}{2} \sum_n (C_1 |u_n - u_{n-1}|^2 + C_2 |u_n - u_{n-2}|^2 - |u_n|^4), \quad (1)$$

where u_n is the dimensionless amplitude of the field in the n -th waveguide.

The propagation of the light field in the current system is governed by the DNSE, which can be obtained by $id u_n/dz = \partial H/\partial u_n^*$ as

$$i \frac{d}{dz} u_n = -\frac{C_1}{2} (u_{n+1} + u_{n-1} - 2u_n) - \frac{C_2}{2} (u_{n+2} + u_{n-2} - 2u_n) - |u_n|^2 u_n, \quad (2)$$

The total power of the field is

$$P = \sum_n |u_n|^2. \quad (3)$$

The stationary soliton solutions of Eq. (2) can be written as

$$u_n(z) = \phi_n e^{i\beta z}, \quad (4)$$

where ϕ_n is the dimensionless amplitude of the soliton and β is the propagation constant. The stability of the localized stationary modes is investigated numerically by means of computing the eigenvalues for small perturbations and is verified by performing direct simulations. The perturbed solution is taken as

$$u_n = e^{i\beta z} (\phi_n + w_n e^{i\lambda z} + v_n^* e^{-i\lambda^* z}), \quad (5)$$

where the asterisk denotes the complex conjugate. Following the substitution of this expression into Eq. (2), linearization leads to the eigenvalue problem for λ and the eigenmodes (w_n, v_n) :

$$\begin{pmatrix} \mathbf{C} + \beta - 2|\phi_n|^2 & \phi_n^2 \\ -\phi_n^{*2} & -\mathbf{C} - \beta + 2|\phi_n|^2 \end{pmatrix} \begin{pmatrix} w_n \\ v_n \end{pmatrix} = \lambda \begin{pmatrix} w_n \\ v_n \end{pmatrix}. \quad (6)$$

where \mathbf{C} is a matrix that defines the total effect of the linear coupling. The elements of \mathbf{C} are defined as

$$C_{ij} = -\frac{1}{2} C_1 (\delta_{i,j-1} + \delta_{i,j+1} - 2\delta_{i,j}) - \frac{1}{2} C_2 (\delta_{i,j-2} + \delta_{i,j+2} - 2\delta_{i,j}), \quad (7)$$

where $\delta_{i,j}$ is the Kronecker symbol. The solution ϕ_n is stable if the spectrum of the eigenvalues λ is real. If we select the waveguide arrays fabricated on AlGaAs, and the real nonlinear parameter and real coupling coefficient are $3.6 \text{ m}^{-1} \text{ W}^{-1}$ and 0.82 mm^{-1} , respectively [7, 33], the unit of the scaled total power, i.e., $P = 1$, is 4.4 kW if the coupling coefficient is normalized to 1 by rescaling the nonlinear strength. The coupling coefficient of $C = 1$ corresponds to a distance of ~ 5 microns between two coupled waveguides [7].

Here, positive and negative values of the coupling constant C_i (where $i = 1$ or 2) indicate that these two linear couplings feature an opposite linear mixing. In the current system, because the two types of coupling are opposite to each other, the coupling constants $C_{1,2}$ satisfy $C_1 \cdot C_2 < 0$. In the next section, we carry out analytical and numerical studies of the stationary discrete solitons in the present system.

III. CHARACTERISTICS OF THE SOLITON

A. Analysis

For convenience, we select $|C_1| = |C_2| = 1$ in Eq. (2). Note again that C_1 represents the coupling between two

adjacent layers and C_2 represents the couplings within the same layer, which can be characterized as cross-coupling and self-coupling, respectively. Linearizing Eq. (2) by the plane wave $u_n = A \exp(i\beta z + iqn)$ (where A is the real amplitude of the plane wave), one can obtain the following dispersion relation for the current system:

$$\beta = C_1 \cos q + C_2 \cos 2q - (C_1 + C_2).$$

Because $C_{1,2}$ manifests opposite types of linear mixing, two types of systems are created when $(C_1, C_2) = (1, -1)$ and $(-1, 1)$, respectively. The dispersion curves in the first Brillouin zone (i.e., $-\pi \leq q \leq \pi$) for these two cases are displayed in Fig. 2.

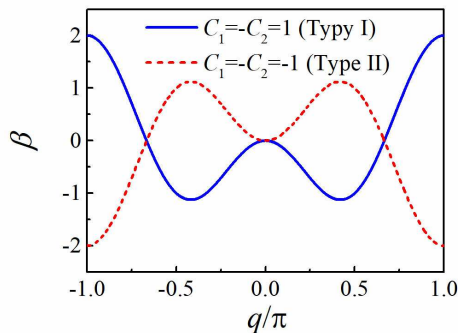


FIG. 2: Dispersion curves for the cases of $(C_1, C_2) = (1, -1)$ (type I, blue solid line) and $(-1, 1)$ (type II, red dashed line).

The dispersion curves indicate that these two types of systems feature opposite dispersion relations at the center (i.e., $q = 0$) and the edge (i.e., $q = \pi$) of the Brillouin zone. At the center of the Brillouin zone, the effective diffraction of the type I array is “normal” (i.e., $\beta''(q)|_{q=0} > 0$), while that of the type II array is “anomalous” (i.e., $\beta''(q)|_{q=0} < 0$). At the edge of the Brillouin zone, the types of effective diffraction are reversed: the type I array becomes “anomalous” (i.e., $\beta''(q)|_{q=\pi} < 0$), and the type II array becomes “normal” (i.e., $\beta''(q)|_{q=\pi} > 0$). Even though the stationary solutions in Eq. (2) are solved only numerically, we can still give some rough analysis of the solitons at the center and edge of the Brillouin zone for the two types of current systems. We assume that the discrete soliton can be written as

$$u_n = A_n e^{i\beta z + iqn},$$

where A_n is the real amplitude and q is equal to 0 or π . At the center of the Brillouin zone (i.e., $q = 0$), the discrete solitons in the type I and type II arrays are described by the following two stationary equations, respectively:

$$-\beta A_n = -\frac{1}{2}(A_{n+1} + A_{n-1}) + \frac{1}{2}(A_{n+2} + A_{n-2}) - A_n^3, \quad (8)$$

$$-\beta A_n = \frac{1}{2}(A_{n+1} + A_{n-1}) - \frac{1}{2}(A_{n+2} + A_{n-2}) - A_n^3. \quad (9)$$

Similarly, at the edge of the Brillouin zone (i.e., $q = \pi$), the discrete solitons in these two types of arrays are described by

$$-\beta A_n = \frac{1}{2}(A_{n+1} + A_{n-1}) + \frac{1}{2}(A_{n+2} + A_{n-2}) - A_n^3, \quad (10)$$

$$-\beta A_n = -\frac{1}{2}(A_{n+1} + A_{n-1}) - \frac{1}{2}(A_{n+2} + A_{n-2}) - A_n^3. \quad (11)$$

Eqs. (9) and (11) can be equivalent to discrete solitons at the edge ($q = \pi$) and center ($q = 0$) of the Brillouin zone of zigzag waveguide arrays with $C_1 \cdot C_2 > 0$ [20]. Bright solitons in these two cases are staggered and un-staggered, respectively. Eq. (10) can support a bright staggered soliton solution if we apply a transformation of $A_n = -A_n$ [20], which can also be indirectly demonstrated by Fig. 7(c) in Section IV. Moreover, Eq. (10) can support dark (or gray) discrete solitons after such a transformation [20]. To the best of our knowledge, Eq. (8) is never considered for discrete solitons. In the following subsection, we carry out numerical simulations and consider the discrete soliton at the center of the Brillouin zone for both types of systems with $(C_1, C_2) = (1, -1)$ and $(-1, 1)$.

B. Numerical results

Discrete solitons at the center of the Brillouin zone are ground-state solutions, which can be numerically solved by the imaginary-time method (ITM) (a standard algorithm for searching for the ground-state solutions of the nonlinear Schrödinger equation and Gross-Pitaevskii equation) [34, 35]. Two families of discrete solitons can be created through the current system with two types of opposite linear mixing between the nearest-neighbor and next-nearest-neighbor couplings. The characteristics of these two families of discrete solitons for these two types of systems are listed in Table I.

TABLE I: Discrete solitons in the two types of systems

Type	(C_1, C_2)	Description
Type I (Multipeak)	$(1, -1)$	Cross coupling is negative; self coupling is positive.
Type II (Staggered)	$(-1, 1)$	Cross coupling is positive; self coupling is negative.

Typical examples of stable solitons for type I and II systems are displayed in Figs. 3 and 4, respectively. These solitons exhibit different characteristics in terms of their amplitudes and intensities. The intensity of the soliton in the type I system features a multipeak structure, while that of the soliton in the type II system features a single-peak structure. The amplitudes of the soliton in the type I system show a π phase shift between two

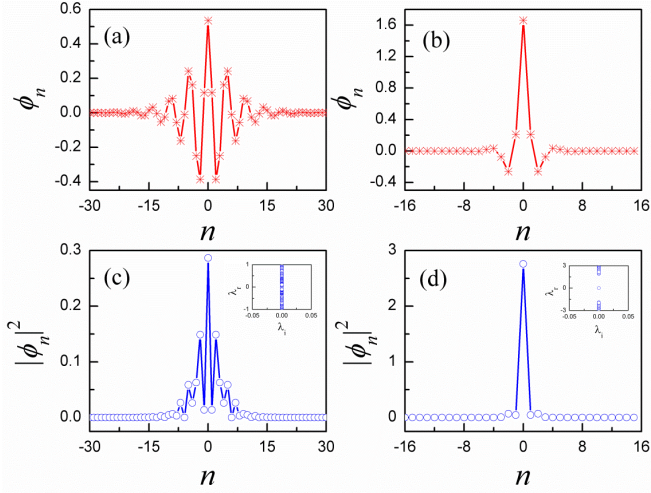


FIG. 3: Typical example of the discrete soliton in the current system with $(C_1, C_2) = (1, -1)$ (type I system). (a,b) Amplitudes of the soliton with $P = 1.0$ and 3.0 , respectively. (c,d) Intensities of the soliton in panels (a,b), respectively. The insets are the spectra of λ , which demonstrate the stabilities of these solitons.

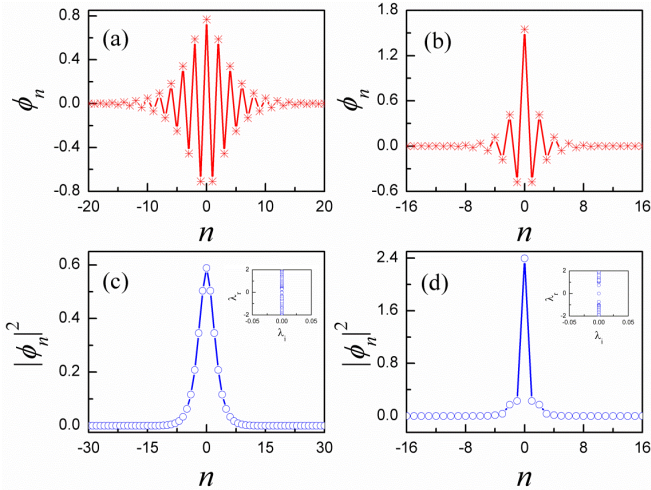


FIG. 4: Typical example of the discrete soliton in the current system with $(C_1, C_2) = (-1, 1)$ (type II system). (a,b) Amplitudes of the soliton with $P = 3.2$ and 3.3 , respectively. (c,d) Intensities of the soliton in panels (a,b), respectively. The insets are the spectra of λ , which demonstrate the stabilities of these solitons.

adjacent peaks, while the soliton in the type II system display a staggered structure at each lattice site (which is in accordance with the analysis in the above subsection). Without considering the next-nearest-neighbor coupling, a π phase shift for peaks or staggered discrete solitons always exists for lattice gap solitons or discrete solitons with self-defocusing Kerr nonlinearity. Here, we observe them in the self-focusing Kerr nonlinearity via the current system. Note that the staggered solitons in the cur-

rent system are different from their counterparts in Ref. [20], which are created at the edge of the Brillouin zone (i.e., $q = \pi$); in contrast, the current staggered solitons are created at the center of the Brillouin zone (i.e., $q = 0$), which results in a zigzag waveguide array with opposite linear mixing between the two types of coupling. If we continue to increase the power, the energy of the field shrinks to the scale of a single waveguide, and the two families of solitons become similar.

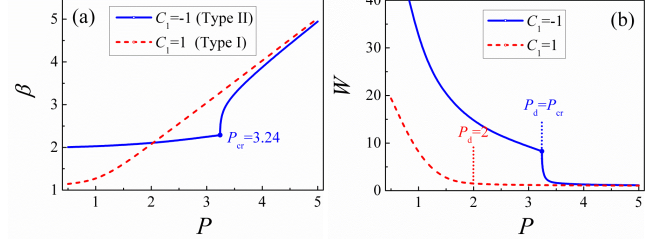


FIG. 5: (a) Propagation constant β of the soliton versus P . The solid blue dot ($P = P_{cr}$) on the curve $\beta(P)$ of the type II soliton indicates the phase transition point. (b) Width of the soliton versus P . The two vertical dotted lines with $P = P_d$ are the borders between the mobile and immobile solitons for the two types of discrete solitons. On the left side of the dotted line ($P < P_d$), the soliton is mobile, while on the right side of the dotted line ($P > P_d$), the soliton becomes immobile. Specifically, for the type II soliton, $P_d = P_{cr}$.

To study the characteristics of the soliton more clearly, we plot the propagation constant β and the effective width as functions of P for the two families of solitons in Fig. 5, where the effective width of the soliton is defined as

$$W = \frac{(\sum_n |u_n|^2)^2}{\sum_n |u_n|^4}.$$

The curves of $\beta(P)$ in Fig. 5(a) for the two families of solitons show that they satisfy the Vakhitov-Kokolov (VK) criterion, i.e., $d\beta/dP > 0$, a necessary stability condition for solitons in self-focusing media. The curve of $\beta(P)$ for the soliton in the type II system reveals that a phase transition for this kind of soliton occurs as P is increases, and the phase transition point is located at $P_{cr} = 3.24$. The behavior of the curve near the phase transition point indicates that this phase transition is of the second kind. Unlike the curve of the soliton in the type II system, the curve of the soliton in the type I system is smooth, which indicates that a phase transition is not detected as P is increases. Fig. 4 displays a typical example of the soliton in the type II system before and after the phase transition. Before the phase transition (i.e., $P < P_{cr}$), the intensity profile of the soliton has a Gaussian shape [see Fig. 4(c)], which are similar to the solitons in a continuous system; the solitons in this case can be regarded as quasi-continuous type. After the phase transition (i.e., $P > P_{cr}$), the intensity profile of

the soliton is different from that of the soliton before the phase transition. The majority of the power of the soliton shrinks to the central site, which gives rise to a substrate around the central site [see Fig. 4(d)]. Then, the curve of $\beta(P)$ of the soliton in the type II system approaches its counterpart in the type I system after the phase transition.

The curves of $W(P)$ in Fig. 5(b) for the two families of solitons show that $W(P)$ decreases as P increases, which can be naturally understood by the feature of the solitons in self-focusing Kerr media. A phase transition is also evident from the curve of $W(P)$ for the soliton in the type II system, which demonstrates that the width of the soliton decreases steeply after the phase transition (i.e., $P > P_{\text{cr}}$).

IV. DYNAMICS OF THE DISCRETE SOLITONS

A. Mobility of the solitons

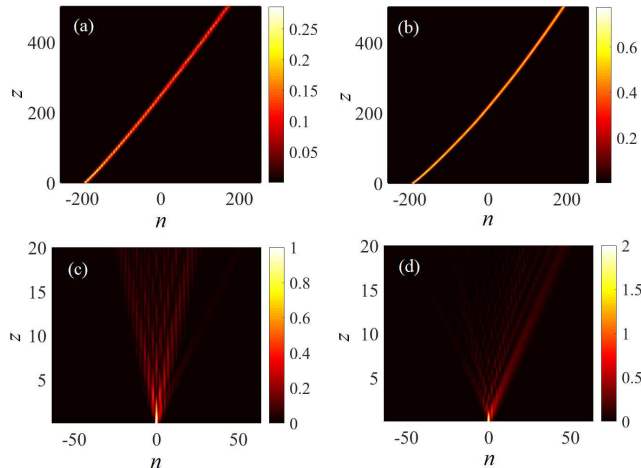


FIG. 6: (a) Motion of a discrete soliton in the type I system with $P = 1$. (b) Motion a discrete soliton in the type II system with $P = 3.2$. The strengths of the kicks in panels (a,b) are $\eta = 0.1\pi$. (c) The discrete soliton in the type I system with $P = 2.2$ is destroyed by the strong kick. (d) The discrete soliton in the type II system with $P = 3.3$ is destroyed by the strong kick. The strengths of the kick in panels (c,d) are $\eta = 0.3\pi$.

Studying the motion of discrete solitons in a discrete system is a nontrivial issue for understanding the dynamic of the discrete solitons. However, how to move a soliton in a discrete lattice while conserving its shape remains unclear. Many papers have discussed this issue; to date, it has been found that the width of a discrete soliton strongly influences its mobility [36–38]. Specifically, if a discrete soliton has a sufficiently broad width (and thus can be termed a quasi-continuous object), the soliton can be more easily mobilized and can be partially explained by the Ablowitz-Ladik model [39].

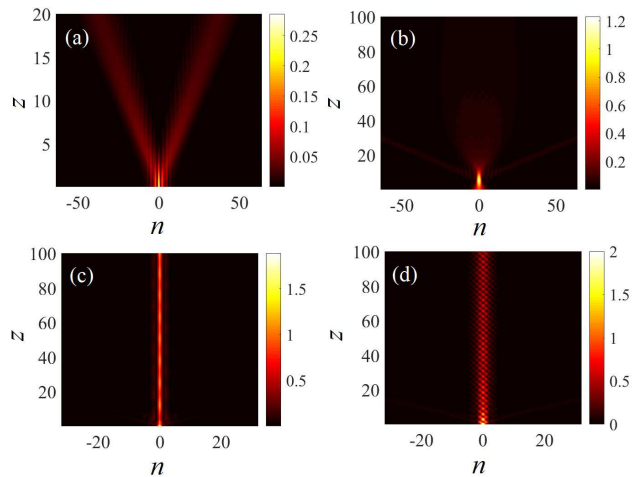


FIG. 7: (a,b) Direct simulations of the solitons in the type I and type II systems with $P = 1$ and $P = 3.2$, respectively, which are all smaller than P_d , kicked by $\eta = \pi$. (c,d) Direct simulations of the soliton in the type I and type II systems with $P = 2.2$ and $P = 3.3$, respectively, which are all larger than P_d , kicked by $\eta = \pi$.

In this paper, the motion of the discrete soliton in the current system is studied by exerting a kick on the stationary solution as

$$u_{n,z=0} = \phi_n e^{i\eta n},$$

where η is the strength of the kick, which can be realized by imprinting a phase tilt on each waveguide (for example, using a spatial light modulator for the waveguide). The numerical algorithm that is employed to study the dynamics of the kicked soliton is the 4-step Runge-Kutta method.

The numerical simulations reveal that the soliton in the type I system can be mobilized in the region where the total power P satisfies $dW/dP < 0$. In this region, the soliton can be moved with a kick if $\eta > \eta_c$, where η_c increases as P increases. A typical example for the moving soliton in this case is depicted in Fig. 6(a). When the total power of the soliton is within the region of $dW/dP \sim 0$, η_c becomes very large, and the soliton is destroyed under the strong kick. This result implies that the solitons are immobile in this region. A typical example of the soliton destroyed by the strong kick in this case is illustrated in Fig. 6(c). For the soliton in the type II system, the numerical simulations show that the soliton can be mobilized before the phase transition ($P < P_{\text{cr}}$), whereas the soliton becomes immobile and is pinned down after the phase transition ($P > P_{\text{cr}}$). If the strength of the kick is small, the soliton cannot be moved by the kick, while if the strength of the kick is large, the kick will destroy the soliton. Typical examples of moving and destroyed solitons are displayed in Fig. 6(b,d).

Based on the above description, the mobilities of the two types of solitons can be clearly identified via the

curves of $W(P)$ in Fig. 5(b). In Fig. 5(b), the solitons on the left side of the vertical dotted line can be mobilized, while the solitons become immobile (or destroyed) on the right side of the vertical dotted line. For convenience, we define the location of the dotted line as $P = P_d$. For the type I soliton, $P_d = 2.0$, while for the type II soliton, $P_d = P_{cr} = 3.24$. Consequently, the discrete soliton in the current system can be mobilized when $P < P_d$, while the soliton cannot be moved by a kick; alternatively, the soliton can be destroyed by exerting kicks of different strengths. Because moving solitons exist on the left side of the vertical dotted line, it is implied that solitons with a larger width can be mobilized more easily than narrower width solitons, which follows from the traditional discrete system. However, the border between mobile and immobile solitons is easier to distinguish in the current system than in traditional discrete systems.

Having a kick of strength $\eta = \pi$, is equivalent to mapping the solitons in the center of the Brillouin zone to the edge of the Brillouin zone. Under this circumstance, two families of solitons with $P < P_d$ and $P > P_d$ exhibit different behaviors. When $P < P_d$, the two families of solitons are destroyed by implementing such a kick; typical examples for this case are shown in Fig. 7(a,b). When $P > P_d$, the two families of solitons can remain localized and propagate in a straight direction by exerting such a kick. This result implies that a soliton solution may exist for both types of systems at the edge of the Brillouin zone.

B. Collision between moving solitons

Another nontrivial issue for the dynamics of the discrete soliton is considering the collision between two moving solitons. Generally, the initial states for both moving solitons can be constructed as

$$u_{n,z=0} = \phi_{n+n_0} e^{i\eta(n+n_0)} + \phi_{n-n_0} e^{-i\eta(n-n_0)},$$

where $\phi_{n\pm n_0}$ denotes the stationary solutions centered at $n = \mp n_0$. The collisions between moving solitons are studied via the soliton that can be mobilized (i.e., $P_{\pm n_0} < P_d$). Because the width of the moving soliton is relatively large, we need to select a sufficiently large n_0 to prevent unnecessary overlap between the two solitons. The numerical simulations show that the properties of the colliding soliton pairs for both types of solitons are strongly influenced by the relationship between $P_{\pm n_0}$ and P_d . If $P_{+n_0} + P_{-n_0} < P_d$, quasi-elastic collisions are observed between soliton pairs. However, if $P_{+n_0} + P_{-n_0} > P_d$, inelastic collisions may be excited. This phenomenon can be explained as follows: when the total power of the colliding solitons exceeds P_d , the solitons may become immobile when they meet and merge together, which results in an inelastic collision. Typical examples of these two collisions for the two types of solitons are displayed in Fig. 8.

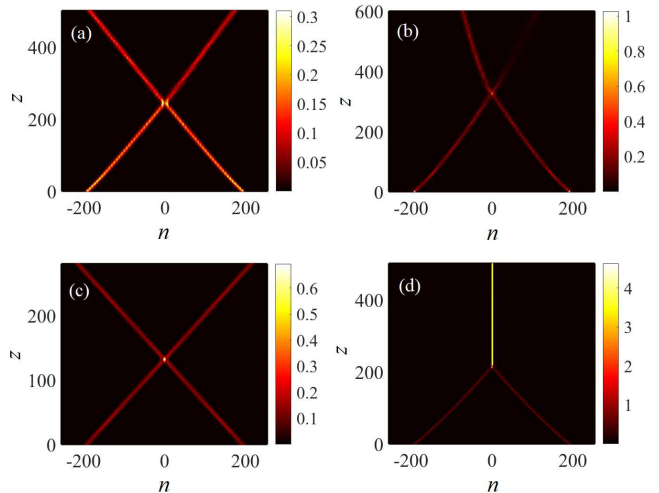


FIG. 8: Typical examples of colliding solitons. (a) Elastic collision between two type I solitons with $P_{\pm n_0} = 1$, where $\eta = 0.1\pi$. (b) Inelastic collision between two type I solitons with $P_{\pm n_0} = 1.5$, where $\eta = 0.15\pi$. (c) Elastic collision between two type II solitons with $P_{\pm n_0} = 1.5$, where $\eta = 0.1\pi$. (d) Inelastic collision between two type II solitons with $P_{\pm n_0} = 3.2$, where $\eta = 0.1\pi$. Here, we select $n_0 = 192$ for all of the panels.

V. CONCLUSIONS

The objective of this work is to study the characteristics and dynamics of discrete solitons in zigzag waveguide arrays that feature different types of linear mixing between nearest-neighbor and next-nearest-neighbor couplings. Two families of discrete solitons are found in two types of waveguide systems, where the nearest-neighbor coupling and the next-nearest-neighbor coupling feature opposite relationships (i.e., $C_1 \cdot C_2 < 0$). The type I system is formed when the nearest-neighbor and next-nearest-neighbor couplings feature negative and positive linear mixing, respectively, while the type II system is formed when the nearest-neighbor and next-nearest-neighbor couplings feature linear mixing opposite to those of the type I system. The dispersion relations for these two types of settings are analyzed by linearizing the system through the plane wave approximation, and the characteristics of the soliton are studied by numerical simulation. The solitons in the type I system have a multipeak intensity profile, and a π phase shift exists for two adjacent peaks of a soliton. The solitons in the type II system are staggered solitons. Interestingly, a phase transition of the second kind occurs as the total power of the soliton increases in the type II system. Furthermore, the phase transition point, P_{cr} , is clearly identified. Before the phase transition, the intensity profile of the soliton in the type II system has a Gaussian shape; after the phase transition, the majority of the power of the soliton shrinks at the central point. Moreover, the mobilities of the two families of solitons are studied throughout the

paper. The solitons in the current systems can be mobilized when their total power satisfies $P < P_d$, and the solitons become immobile (pinned down or destroyed under different kick strengths) when $P > P_d$. The values of P_d for the two types of solitons are identified in this paper. For the soliton in the type I system, P_d is the border between the regions satisfying $dW/dP < 0$ (where W is the effective width of the soliton) and $dW/dP \sim 0$. For the solitons in the type II system, $P_d = P_{cr}$. Collisions between moving solitons are also discussed. An elastic collision is obtained if the total power of the solitons is smaller than P_d when the solitons merge; otherwise, an inelastic collision occurs.

Synthetic gauge fields and discrete matter-wave solitons are active research topics and attract considerable interest in the field of Bose-Einstein condensates [40–49]. The discussion in this paper is also suitable for a matter-wave soliton trapped in a zigzag optical lattice with the same competition between the two types of coupling (i.e.,

the hopping rate).

VI. ACKNOWLEDGMENTS

This work was supported by the NNSFC (China) through grant Nos. 11905032, 11874112, and 11575063, the Foundation for Distinguished Young Talents in Higher Education of Guangdong through grant No. 2018KQNCX279, Key Research Projects of General Colleges in Guangdong Province through grant No. 2019KZDXM001.

Declaration of competing interest

The authors declare that they have no known competing financial interests or personal relationships that could have appeared to influence the work reported in this paper.

-
- [1] I.L. Garanovich, S. Longhi, A.A. Sukhorukova, and Y.S. Kivshar, *Phys. Rep.* **518** (2012) 1.
 - [2] D.N. Christodoulides, F. Lederer, and Y. Silberberg, *Nature* **424** (2003) 817.
 - [3] H.S. Eisenberg, Y. Silberberg, R. Morandotti, J.S. Aitchison, *Phys. Rev. Lett.* **85** (2000) 1863.
 - [4] Y. Lahini, A. Avidan, F. Pozzi, M. Sorel, R. Morandotti, D.N. Christodoulides, and Y. Silberberg, *Phys. Rev. Lett.* **100** (2008) 013906.
 - [5] T. Pertsch, P. Dannberg, W. Elflein, A. Brauer, F. Lederer, *Phys. Rev. Lett.* **83** (1999) 4752.
 - [6] F. Lederer, G.I. Stegemanb, D.N. Christodoulides, G. Assanto, M. Segev, and Y. Silberberg, *Phys. Rep.* **463** (2008) 1.
 - [7] H.S. Eisenberg, Y. Silberberg, R. Morandotti, A.R. Boyd, and J.S. Aitchison, *Phys. Rev. Lett.* **81** (1998) 3383.
 - [8] R. Morandotti, U. Peschel, J.S. Aitchison, H.S. Eisenberg and Y. Silberberg, *Phys. Rev. Lett.* **83** (1999) 2726.
 - [9] X. Zhang, J. Chai, J. Huang, Z. Chen, Y. Li, and B.A. Malomed, *Opt. Express* **22** (2014) 13927.
 - [10] Z. Chen, J. Huang, J. Chai, X. Zhang, Y. Li, and B.A. Malomed, *Phys. Rev. A* **91** (2015) 053821.
 - [11] C.Q. Dai, J.F. Zhang, *International Journal of Modern Physics B* **19** (2005) 2129.
 - [12] C.Q. Dai and Y.Y. Wang, *Phys. Scr.* **78** (2008) 015013.
 - [13] M. Li, J. Shui, T. Xu, *Appl. Math. Lett.* **83** (2018) 110.
 - [14] T. Xu, H. Li, H. Zhang, M. Li, S. Lan, *Appl. Math. Lett.* **63** (2017) 88.
 - [15] F. Ye, L. Dong, J. Wang, T. Cai and Y. Li, *Chinese Optics Letters* **3** (2005) 227.
 - [16] Z. Yan, *Appl. Math. Lett.* **22** (2009) 448.
 - [17] A.V. Yulin and D.V. Skryabin, A.G. Vladimirov, *Opt. Express* **14** (2006) 12347.
 - [18] A.V. Yulin, A.R. Champneys, and D.V. Skryabin, *Phys. Rev. A* **78** (2008) 011804.
 - [19] D.N. Christodoulides and E.D. Eugenieva, *Phys. Rev. Lett.* **87** (2001) 233901.
 - [20] N.K. Efremidis and D.N. Christodoulides, *Phys. Rev. E* **65** (2002) 056607.
 - [21] P.G. Kevrekidisa, B.A. Malomed, A. Saxena, A.R. Bishop, D.J. Frantzeskakis, *Physica D* **183** (2003) 87.
 - [22] A. Szameit, R. Keil, F. Dreisow, M. Heinrich, T. Pertsch, S. Nolte, and A. Tünnermann, *Opt. Lett.* **34** (2009) 2838.
 - [23] C.Chong, R. Carretero-González, B.A. Malomed, P.G. Kevrekidis, *Physica D* **240** (2011) 1205.
 - [24] A.A. Dovgij and I.S. Besedin, *Phys. Rev. E* **92** (2015) 032904.
 - [25] Z. Mai, S. Fu, J. Wu, and Y. Li, *J. Phys. Soc. Jpn.* **83** (2014) 034404.
 - [26] Z. Mai, W. Pang, J. Wu, and Y. Li, *J. Phys. Soc. Jpn.* **84** (2015) 014401.
 - [27] Y. Lumer, M.A. Banders, H.H. Sheinfux, Y. Plotnik, M. Heinrich, A. Szameit, M. Segev, *Nat. Photonics* **13** (2019) 339.
 - [28] H. Huang, X. Zhu, S. Su, H. Li, C. Huang, H. Lin, Z. Chen, *J. Nonlinear Opt. Phys. & Mat.* **26** (2016) 1750012.
 - [29] K. Fang, Z. Yu, and S. Fan, *Nat. Photonics* **6** (2012) 782.
 - [30] M. Golshani, S. Weimann, Kh. Jafari, M.K. Nezhad, A. Langari, A.R. Bahrapour, T. Eichelkraut, S.M. Mahdavi, and A. Szameit, *Phys. Rev. Lett.* **113** (2014) 123903.
 - [31] A.G. Ardakani, *Appl. Opt.* **55** (2016) 3589.
 - [32] M.K. Nezhad, M. Golshani, D. Mirshamsia, *Opt. Communications* **405** (2017) 387.
 - [33] J. S. Aitchison, D. C. Hutchings, J. U. Kang, G. I. Stegeman, and A. Villeneuve, *IEEE J. Quantum Electron.* **33**, (1997) 341.
 - [34] L.M. Chiofalo, S. Succi, and P.M. Tosi, *Phys. Rev. E* **62** (2000) 7438.
 - [35] J. Yang and T.I. Lakoba, *Stud. Appl. Math.* **120** (2008) 265.
 - [36] Y.V. Kartashov, V.A. Vysloukh, and L. Torner, *Progress in Optics* **52** (2009) 63.
 - [37] J. Huang, H. Li, X. Zhang, Y. Li, *Front. Phys.* **10** (2015) 104201.
 - [38] Z. Peng, H. Li, Z. Fan, X. Zhang and Y. Li, *J. Nonlinear Opt. Phys. & Mat.* **24** (2015) 1550022.

- [39] D. Cai, A.R. Bishop, N. Grønbech-Jensen, and B.A. Malomed, *Phys. Rev. E* **50** (1994) R694.
- [40] A. Trombettoni and A. Smerzi, *Phys. Rev. Lett.* **86** (2001) 2353.
- [41] V. Ahufinger, A. Sanpera, P. Pedri, L. Santos, and M. Lewenstein, *Phys. Rev. A* **69** (2004) 053604.
- [42] M. Atala, M. Aidelsburger, M. Lohse, J.T. Barreiro, B. Paredes, and I. Bloch, *Nat. Phys.* **10** (2014) 588.
- [43] R. Wei and E.J. Mueller, *Phys. Rev. A* **89** (2014) 063617.
- [44] G. Gligorić, A. Maluckov, L. Hadžievski, and B.A. Malomed, *Phys. Rev. A* **78** (2008) 063615.
- [45] H. Chen, Y. Liu, Q. Zhang, Y. Shi, W. Pang, and Y. Li, *Phys. Rev. A* **93** (2016) 053608.
- [46] Z. Fan, Y. Shi, Y. Liu, W. Pang, Y. Li, and B.A. Malomed, *Phys. Rev. E* **95** (2017) 032226.
- [47] Y. Li, Z. Fan, Z. Luo, Y. Liu, H. He, J. Lü, J. Xie, C. Huang, H. Tan, *Front. Phys.* **12** (2017) 124206.
- [48] Q. Ye, X. Qin, Y. Li, H. Zhong, Y.S. Kivshar, C. Lee, *Annals of Physics* **388** (2018) 173.
- [49] X. Zhang, X. Xu, Y. Zheng, Z. Chen, B. Liu, Ch. Huang, B.A. Malomed, and Y. Li, *Phys. Rev. Lett.* **123** (2019) 133901.